Technical Paper

ISSN 1997-1400 Int. J. Pavement Res. Technol. 7(4):263-272

A Study on Cross-anisotropy of Unbound Layers of Pavement Considering Nonlinearity

Mesbah U. Ahmed[1+], Rafiqul A. Tarefder[1], M. Rashadul Islam[1], and M. Tahmidur Rahman[1]

Abstract: The effects of cross-anisotropy of unbound layer materials on the stress-strain response of a pavement under Falling Weight Deflectometer (FWD) test load are determined at three temperatures employing a dynamic Finite Element Model (FEM) in ABAQUS. Viscoelastic behavior of Asphalt Concrete (AC) is characterized by laboratory dynamic modulus test. Nonlinear elasticity of base material is incorporated through a User Defined Material (UMAT) subroutine. Cross-anisotropy is introduced by changing the ratio of horizontal to vertical stiffness (*n*-value) of unbound layers. FEM model is validated using field collected stress-strain under FWD test on the instrumented pavement section at mile post 141 (MP 141) on Interstate 40 (I-40) near Albuquerque, New Mexico. It is observed that tensile strain at the bottom of the AC layer is influenced by the base layer cross-anisotropy whereas vertical strain in this layer is barely affected by the cross-anisotropy of the unbound layers. However, vertical strains in the unbound layers are significantly affected by cross-anisotropy. Therefore, it can be postulated that fatigue damage by tensile strain at the bottom of AC layer, and rutting by vertical strain should be evaluated for unbound layer cross-anisotropy in the pavement design. Overall, strain responses due to cross-anisotropy are highly sensitive to temperature.

DOI: 10.6135/ijprt.org.tw/2014.7(4).263
Key words: Asphalt pavements; Anisotropy; Dynamic analysis; FEM.

Introduction

Pavement material stiffness in the horizontal direction may vary from the vertical direction due to vertical compaction during construction followed by the repetition of vertical wheel loads in service [1]. The ratio of stiffness or modulus of elasticity (*E*-value) along horizontal to vertical directions is defined as *n*-value, which is used to define material isotropy ($n=1$) and anisotropy ($n\neq1$). Cross-anisotropy is a special case of anisotropy in which *E*-values along horizontal directions (i.e., lateral and longitudinal) are considered equal [2-4]. In addition, temperature is another important factor that affects stiffness (*E*-value) of pavement materials [5-7]. Generally, the Asphalt Concrete (AC) modulus is high at low temperature whereas it is low at high temperature [8]. This study focuses on the combined effects of cross-anisotropy and temperature on strains of a pavement.

To this day, a number of studies have been performed to address the material cross-anisotropy, and thermal effect separately or together considering either linear or nonlinear elasticity under static or dynamic loading [2, 3, 9-11]. In the static loading group, Masad et al. [2] developed both isotropic and anisotropic material models to determine the pavement response through an axisymmetric Finite Element Model (FEM) under static Benkelman beam load**.** Oh et al. [11] developed four different cross-anisotropy material models implemented by a static FEM to determine the pavement response under Falling Weight Deflectometer (FWD) and multi-depth deflectometer test. Choi et al. [9] developed a 3D static FEM using anisotropic behavior of AC and base layer with nonlinearity. A temperature distribution with depth is integrated to this model. The AC property variation with temperature was not documented in their study.

In the dynamic loading group, Al-Qadi et al. [10] investigated the cross-anisotropic effect of the unbound layers with nonlinearity using 3D dynamic FEM with implicit algorithm to simulate FWD test results. Howard and Warren [12] developed an axisymmetric FEM to determine the response of an instrumented pavement section under dynamic load, however, did not consider material cross-anisotropy. Ahmed et al. [3] investigated the effect of material cross-anisotropy under dynamic loading, however, did not consider the temperature variation. Only very recently, Wang and Al-Qadi [4] developed a dynamic FEM to examine the effect of cross-anisotropy in the nonlinear unbound layer (base) at two different temperatures such as 25℃ and 47℃.

From the above discussions, it is clear that the effects of material cross-anisotropy, pavement temperature, and material nonlinearity were studied under dynamic loading in FEM framework. What has not been done is the study of the effects of cross-anisotropy at a wider temperature range, and multiple layers such as base, subbase, and subgrade. To this end, this study determines the effects of cross-anisotropy of base, subbase, and subgrade subjected to three different temperatures and dynamic loading, by FWD test load, on the strain values in a dynamic FEM framework.

Objectives

The main objective of this study is to investigate the effects of unbound layer cross-anisotropy on pavement response such as horizontal strain at the bottom of the AC layer and vertical strains in all the layers (AC, base, subbase, and subgrade) under FWD test load at different temperature in AC layer. In this study, average

[1] Dept. of Civil Engineering, University of New Mexico, Albuquerque, NM 87131-0001, USA.
[+] Corresponding Author: E-mail mahmed@unm.edu
Note: Submitted January 8, 2014; Revised June 14, 2014; Accepted June 16, 2014.

temperature over the depth of AC layer is considered as AC layer temperature.

Dynamic Finite Element Modeling

Model Geometry

The geometry of the FEM is constructed based on an instrumented pavement section at mile post 141 (MP 141) on Interstate 40 (I-40) as shown in Fig. 1. It consists of four layers: AC at the surface, aggregate layer at the base, Process-Place and Compacted (PPC) layer at the subbase, and a subgrade soil layer. The PPC layer is prepared by processing (disintegrating) existing base and/or subgrade materials and then, compacting it in place. The AC layer consists of three lifts each with a thickness of 8.89 cm (3.5 in.). The thickness of the base is 15.24 cm (6 in.) and the subbase is 20.32 cm (8 in.). From Fig. 1, it can be seen that horizontal asphalt strain gauges (HASGs) and vertical asphalt strain gauges (VASGs) were installed at the bottom and inside of the AC layer respectively. Earth pressure cells were installed at different depths to measure the vertical stress.

Mesh Generation

A model is selected for mesh generation as shown in Fig. 2(a). An 8-noded brick element is used for the mesh generation. However, the region enclosed by the loading area at the top of the AC layer (3.5 in.) is meshed using a combination of 6-noded wedge element (C3D6) and 8-noded brick element (C3D8) to facilitate the circular (FWD) loading area. A coarse mesh is used in the region far from the loading area. An edge biased structure meshing pattern available in ABAQUS is used to obtain a smooth transition from fine mesh to coarse mesh.

Typically, a FEM dynamic simulation with 3D model requires very high memory space as well as analysis time [13]. A quarter cube model is used for a 3D simulation to reduce the memory space and analysis run time since it has two axis of symmetry. Wave reflection by the boundary is one of the major concerns in a dynamic analysis. Dynamic amplification may occur due to this wave reflection that results from the insufficient distance to the boundary [14]. According to Duncan et al. [15], depth and horizontal length of the model should be sufficient to ignore this effect due to the insufficient distances to boundaries. In this study, following Duncan et al. [15], depth of the model was taken 50 times the loading radius and horizontal length was taken more than 12 times the loading radius. Final dimensions, i.e., length, width, and depth, of this entire model are 5.08 m x 5.08 m x 7.62 m (200 in. x 200 in. x 300 in.). However, length of the model (200 in.) is checked for any possible wave reflection from the vertical boundary. The compressive wave propagation speed is determined from the bulk modulus and density of AC material (see section Material Properties). Travel time of wave propagation is then determined from the ratio of length of the model and the calculated compressive wave propagation speed. It is observed that the wave travel time is greater than twice the loading duration (see section Load). It indicates that the wave does not reach the boundary before the loading duration ends. Therefore, there is no possibility of wave

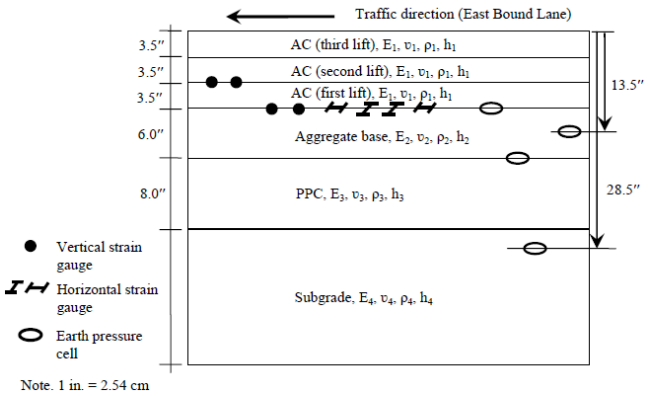

Fig. 1. Instrumented Section.

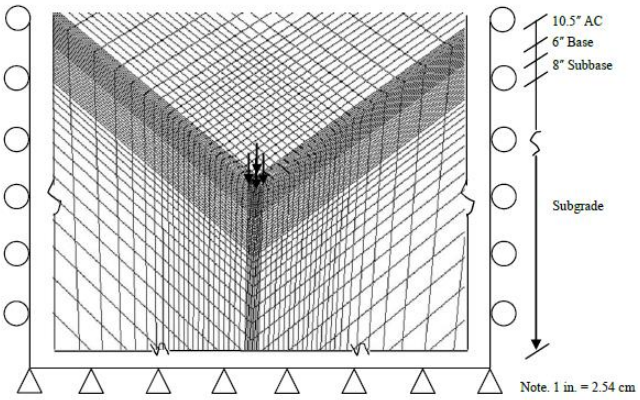

(a) Mesh over the model

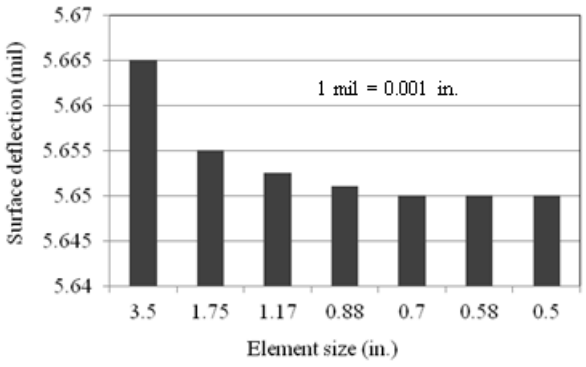

(b) Mesh sensitivity

Fig. 2. Mesh Generation and Boundary Condition

reflection from the boundary. The number of layers as well as thicknesses of every layer is assigned according to the instrumented section described earlier.

The size of the element during the mesh generation is selected after a number of trial analyses during a mesh-sensitivity analysis (see Fig. 2(b)). The mesh-sensitivity analysis is performed by simulating the dynamic FEM for varying sizes of elements. The element size near the loading area is varied due to the influence of these elements on the stress gradient. In essence, a number of simulations were performed by reducing the depth of elements in AC layer from 89 mm (3.5 in.) to 13 mm (0.5 in.). From each of the simulations, vertical surface deflection is determined at the node that coincides with the center of the load. The effect of the element

size variation on the vertical surface deflection shows that the deflection diminishes with gradual reduction of the depth of this element. The trend of vertical deflection with element depth variation begins to be constant from the simulation with the element depth of 18 mm (0.7 in.). Based on the consideration of accuracy, analysis time and memory storage for the dynamic simulations, the optimum depth of the smallest element is found to be 18 mm.

Boundary Condition

The bottom boundary is restrained to move along the three mutually orthogonal directions (see Fig. 2(a)). Therefore, there will be no deflection in horizontal and vertical directions on bottom boundary. Movements of the vertical planes are restrained only in the horizontal directions. The instrumented pavement section has been constructed very recently. In addition, this study has been initiated to perform right after the construction. Moisture or other climatic conditions has not delaminated the bonding at interfaces of different layers within this short period of time. Therefore, two consecutive layers with different types of materials at the interface are assumed to be fully bonded.

Material Properties

Materials' properties are determined through field and laboratory testing.

AC Layer Properties

All three lifts of AC were constructed using SuperPave (SP), Type-III mix, which uses nominal aggregate size of 19.0 mm (0.75 in.). Therefore, these layers are reasonably assumed to have the identical property, represented by linear viscoelastic material [16-18]. AC cores were collected from the field and dynamic modulus testing was conducted according to the AASHTO TP 62-07 [19] procedure.

Dynamic modulus master curve was generated from test data at different temperatures (-10, 4, 21, 37, and 54°C) and frequencies (0.1, 0.5, 1, 5, 10 and 25 Hz). The master curve was used to determine the coefficients of the Prony series that represent the viscoelastic behavior of AC in FEM model. Determination of these coefficients involves two steps: one is to determine the relaxation modulus and the other is to determine the Prony series coefficients by fitting the Maxwell model to the relaxation modulus. This conversion is performed according to the method of conversion as proposed by Park and Schapery [20]. The generalized equation is as follows:

$$E(t) = E_0\left[1 - \sum_{i=1}^{N} e_i\left(1 - e^{-t/\tau_i}\right)\right] \quad (1)$$

where $E(t)$ = relaxation modulus at time t second (ksi), E_0 = instantaneous modulus (ksi), e_i = Prony series coefficients, τ_i = reduced relaxation time and N = number of Maxwell model. These are summarized in Table 1. In addition, instantaneous moduli of AC (E_0) at different temperatures are documented in Table 2.

Table 1: Viscoelastic Parameters of AC Layer

i	Reduced relaxation time, τ_i	Prony series coefficient, e_i
1	0.00912	0.1
2	0.02	0.1
3	0.05	0.1
4	0.1	0.1
5	0.3	0.09
6	1	0.09

Base Layer

The base layer was constructed using 50% granular aggregate and 50% Recycled Asphalt Pavement (RAP) material. This layer is considered nonlinear elastic in the dynamic FEM of the pavement section. Laboratory resilient modulus test was conducted to determine this nonlinearity of the base material according to the AASHTO T307-99 [21]. The generalized model as adopted in the newly developed Mechanistic Empirical Pavement Design Guide (MEPDG) is used in this study to incorporate base nonlinearity to the model [22]. The model is as below:

$$M_r = k_1 p_a \left(\frac{\theta}{p_a}\right)^{k_2} \left(\frac{\tau_{oct}}{P_a} + 1\right)^{k_3} \quad (2)$$

where θ = bulk stress, τ_{oct} = octahedral shear stress, P_a = atmospheric pressure, and k_1, k_2, k_3 = regression coefficients that need to be determined from laboratory resilient modulus test. The regression coefficients, i.e., k_1, k_2, k_3 of base material were determined from laboratory measured resilient modulus (M_r) at different loading sequences. The values of these coefficients are determined to be 5.006, 0.1387, and 0.9816 respectively. Finally, the equation is:

$$M_r = 5.006 p_a \left(\frac{\theta}{p_a}\right)^{0.1387} \left(\frac{\tau_{oct}}{p_a} + 1\right)^{0.9816} \quad (3)$$

where M_r is in 'ksi' and θ, τ_{oct}, P_a are in 'psi'. Nonlinear property of the base layer is also summarized in Table 2. Eq. (3) is implemented in dynamic FEM using User Defined Material (UMAT) in ABAQUS. In UMAT, for each of base layer elements, the initial strain increments are obtained from the main program to calculate the stresses. These stresses are used to determine the bulk and octahedral stresses, which are used to calculate resilient modulus using Eq. (3). Based on the resilient modulus, the incremental stiffness is calculated and the stress is updated and returned to the main program.

Subbase and Subgrade

Table 2 summarizes the material properties for both subbase and subgrade. In the dynamic FEM, these are assumed linear elastic. Instead of laboratory testing, the layer moduli are backcalculated from FWD test data using a multilayered elastic analysis algorithm. The average backcalculated moduli of the subbase and subgrade used in FEM model are 682.6 MPa (99 ksi) and 172.4 MPa (25 ksi) respectively. Theses backcalculated moduli of subbase and subgrade are assigned as stiffness along vertical directions. Stiffness along horizontal directions for both of the layers is assigned based on

Table 2. Material Parameter.

Parameter	AC		Base	Subbase	Subgrade
Instanteneous Modulus/ k-values/E-value (ksi)	12.3℃ 25.3℃ 33.3℃	1134.78 825.13 543.6	k_1=5.006; k_2=0.1387; k_3=0.9816	99	25
Poisson's Ratio, ν	0.35		0.4	0.4	0.45
Density, ρ (pcf)	145		135	120	110

Note[1]. 1 ksi = 6.89 MPa; Note[2]. 1 pcf = 16.02 kg/m^3

Note[3]. AC requires "Instantaneous modulus", base material requires "k-values", and subbase and subgrade require "k-value"

cross-anisotropic variations.

Cross-Anisotropy

Cross-anisotropy is assigned to layer materials by varying the magnitude of anisotropy parameters such as *n* and *m* defined as follows:

$$n = \frac{E_{11}}{E_{22}} \tag{4}$$

$$m = \frac{G_{12}}{E_{22}} \tag{5}$$

where E_{11}= modulus of elasticity along horizontal plane, E_{22} = modulus of elasticity along vertical plane, and G_{12} = shear modulus of elasticity. For cross-anisotropy, $E_{11} = E_{33}$, where E_{33} = modulus of elasticity on the horizontal plane along the transverse direction. The layer moduli, whether it is determined from the resilient modulus or backcalculated, is assigned as E_{22}. E_{11} and E_{33} are calculated multiplying E_{22} by the *n*-value, which is varied arbitrarily (n = 0.5, 0.75, 1.0). Shear modulus is assumed to be the same over three orthogonal planes. That is, $G_{12} = G_{23} = G_{13} = G$. In this study, *n*-value is varied for the unbound layers: base, subbase, and subgrade. The *m*-value is assumed as 0.38, a constant, according to Kim [23].

Load

FWD load is idealized by a circular area in FEM model. Variation of FWD load over time is shown in Fig. 3. During the FWD test, five replicate drops were applied at the target load of 40.03 kN (9 kip) for repeatability. It generated a vertical stress of 548.8 kPa (79.6 psi) on a circular area of 6 inch radius. The magnitude of load varies over 25 milliseconds, as shown in Fig. 3. The maximum load of 40.03 kN (9 kip) is recorded at 10 milliseconds.

Dynamic FEM Analysis

A pavement section under FWD test load should be considered as a dynamic system because load varies as a function of time. Typically, a dynamic system is idealized by a mass, damper, and a spring subjected to loading. The general equation of a dynamic system can be written as Hagström [24]:

$$M\ddot{u} + C\dot{u} + Ku = F(t) \tag{6}$$

where M = mass of the system, C = damping coefficient, K = stiffness of the system, and $u, \dot{u}, \ddot{u}$= displacement, velocity, and acceleration respectively.

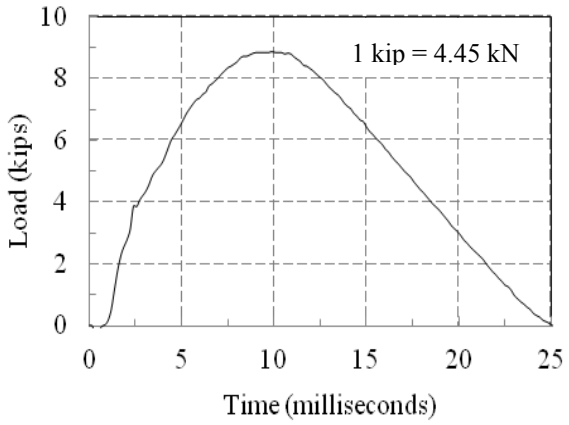

Fig. 3. FWD Test Load Variation Over Time.

There are two algorithms to solve the above differential equation. These are implicit and explicit algorithms [25]. The explicit algorithm solves the equation at a later time from the state of the system at the current time and does not require a long analysis time. However, stability of the explicit algorithm is conditional. On the other hand, the implicit algorithm is unconditionally stable though it requires time. The implicit algorithm solves Eq. (6) using both the current and the later state.

As mentioned earlier, AC is considered to be a viscoelastic material; there is no need to assign any damping to this layer [4]. Damping is assigned to other layers using a Rayleigh damping scheme. According to this scheme, the *C* matrix, as required in Eq. (6), is generated as follows:

$$[C] = \alpha[M] + \beta[K] \tag{7}$$

where [*C*] = damping matrix, [*M*] =mass matrix, [*k*] = stiffness matrix, and α, β = constants for specific damping ratio. These constants are determined using the following relationship:

$$\zeta = \frac{\alpha}{2\omega} + \frac{\beta\omega}{2} \tag{8}$$

where ζ = damping ratio, and $\boldsymbol{\omega}$ = angular frequency of the system.

The damping ratio of 5% is selected for unbound layer materials. Incorporation of damping with the selected damping ratio using the Rayleigh damping scheme is complex since the frequency is unknown [26]. Serdaroglu [27] approach is used to determine the frequencies from the dynamic analysis. In essence, Fast Fourier

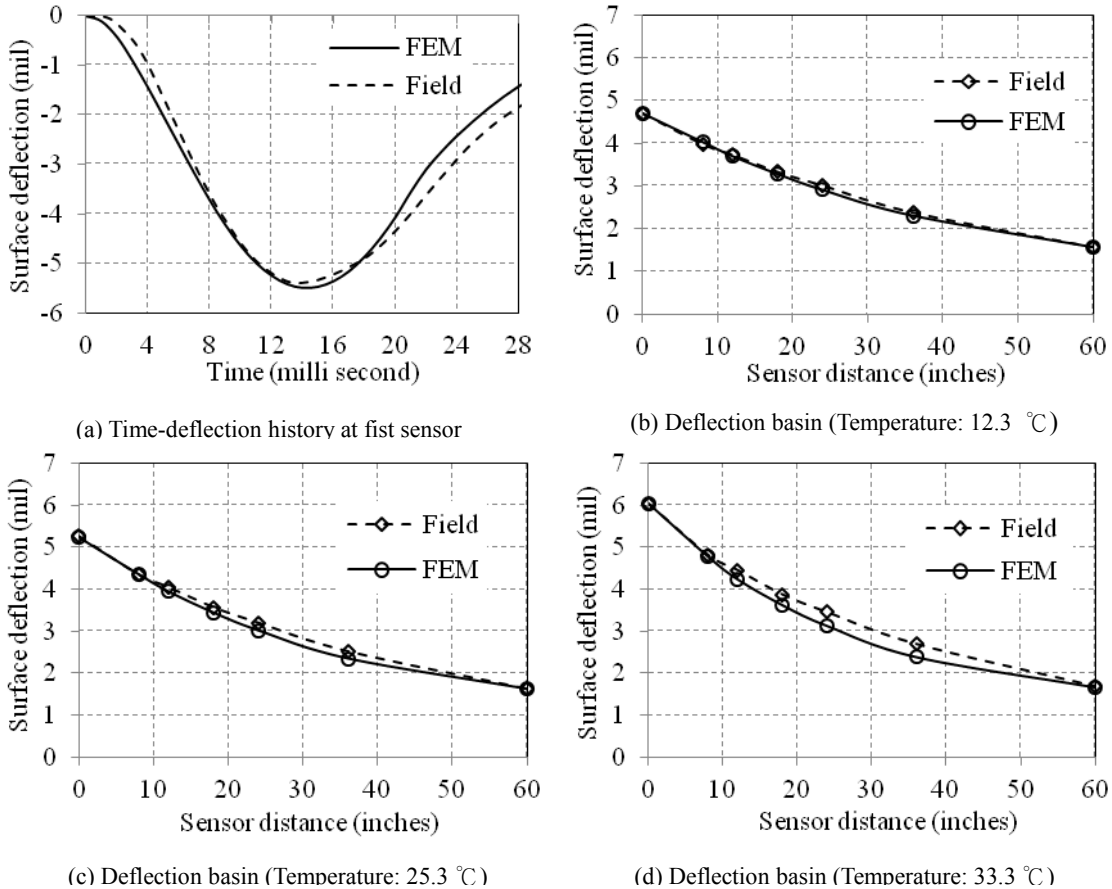

Fig. 4. Model Validation Using FWD Test Data.

Transformation (FFT) was performed on the time history of velocity at the furthest node to determine the frequencies according to this approach. The time history of velocity has been extracted at the furthest node right above the bottom support, i.e., 106.7 cm (42.0 in.) above the bottom or support. Incorporating the frequencies and $\zeta = 0.05$ into the Eq. (8), the values of α and β are 10.0 (1/s) and 0.00025 (s) respectively.

Model Material Inputs

The dynamic FEM simulation is performed for FWD test load at three selected pavement temperatures and *n*-values. For the FEM simulation three major temperatures are selected based on the temperature variation during the spring in New Mexico. These are 12.3°C, 25.3°C, and 33.3°C respectively. These temperatures are calculated by averaging temperature readings from four temperature probes at different depths of the pavement section. These temperature probes have been installed 0, 50, 100, and 300 mm (0, 2, 4, and 12 in.) from the pavement surface. At each of the selected temperatures, the cross-anisotropy parameter is 0.5, 0.75, and 1.0 respectively. The *n*-value is varied in each single layer except the AC layer as well as the combination of three unbound layers during the simulation at different temperatures.

Results and Discussion

Model Validation

Prior to the investigation of temperature dependency and effect of cross-anisotropy, the model was validated with the field measured deflection, stress and strain. FWD test was conducted on the locations of the pavement section (MP 141, I-40), where the HASG and earth pressure cells were installed, over a day to collect data such as deflections, horizontal strain, and stress. During the test at each location, five replicate drops were applied at a target load to ensure the consistent measurement of pavement responses. The time-deflection histories as well as the deflection basin, i.e., peak surface deflections at different sensors, were collected from the test. In addition, the strain and stress data were collected during each of the test drops. This test was conducted in the same sequence at every one hour interval from 9.00 am to 3.00 pm at different pavement surface temperatures.

Fig. 4 compares the field (measured) and FEM (predicted) time-deflection history and peak deflections at the three temperatures. The FEM simulation is performed at the *n*-value of 1 (isotropic). Fig. 4(a) shows that the time-deflection history from the dynamic FEM closely matches with the field time-deflection history. From Fig. 4(b) through 4(d), it can be seen that the surface deflection increases with an increase in pavement temperature. At temperature 12.3°C, the FEM simulated deflection basin closely matches with the field measured deflection basin. The temperature of 12.3°C is calculated from average temperature over the AC layer.

Table 3. Comparison of Tensile Strain and Vertical Stress.

Pavement Temperature (ºC)	Horizontal Strain (με)		Vertical Stress kPa (psi)	
	FEM	Field	FEM	Field
12.3	43.2	41.0	12.89 (1.87)	13.1 (1.90)
25.3	52.3	51.0	14.75 (2.14)	14.48 (2.10)
33.3	65.6	66.0	17.24 (2.50)	15.51 (2.25)

However, there is a slight deviation in deflection values in the mid-sensors at 25.3°C. This deviation is even more at 33.3°C. Overall, the FEM model predicts the peak surface deflection reasonably well, which validates the model.

In addition, the dynamic FEM simulated horizontal strain at the bottom of AC layer (10.5 in. deep from the pavement surface) and vertical compressive stress at 4 in. above the top of the subgrade are compared to the field values. From Table 3, it can be observed that the FEM predictions are very close to field values. The strain as well as the pressure increases with the increase in pavement temperature. This is due to the softening of the AC layer at high temperature. At 12.3°C, the strains from FEM and the field are 43.2 and 41.0 microstrain respectively. At 33.3°C, strains are 65.6 and 66.0 microstrain from FEM and field respectively. Thus, the difference between the Field and FEM simulated strain is very small. In case of vertical stress inside the subgrade, there is no significant difference between FEM and field values. To that end, the developed dynamic FEM was used for cross-anisotropy study under both FWD test loads.

Effect of Cross-Anisotropy on Horizontal Strain

The time-history of the horizontal strain is determined at the bottom of AC layer from the dynamic FEM simulation at different temperatures by varying *n*-values of the unbound layers. The peak strains are obtained from this time-history of horizontal strain. Whenever the *n*-value of an individual unbound layer is varied, the *n*-values of the other layers are kept constant. This type of variation is repeated for base, subbase, and subgrade. In addition to cross-anisotropy variation of individual layer, *n*-values are varied for all the unbound layers together. In this study, it is referred as combined cross-anisotropy variation.

Fig. 5(a) shows the effect of base layer cross-anisotropy on the strain at the bottom of AC layer. At a specific temperature such as 12.3°C, the horizontal strain in AC layer increases gradually with increase in *n*-value. Effect of base layer cross-anisotropy is also investigated at 25.3°C and 33.3°C. The similar trend of horizontal strain variation is observed at these two other temperatures. The exception is that the horizontal strain increases with temperature. This is due to the reduction of AC stiffness at high temperatures. At $n=1$, the change in strain is about 22.44 microstrain increasing from 12.3°C to 33.3°C. This trend is fairly similar for the *n*-values of 0.5 and 0.75. In case of the subbase (PPC) cross-anisotropy, Fig. 5(b) shows that the strain increases with temperature whereas the strain deceases with increase in *n*-value at a certain temperature. This is due to the increase in modulus of elasticity along the horizontal direction.

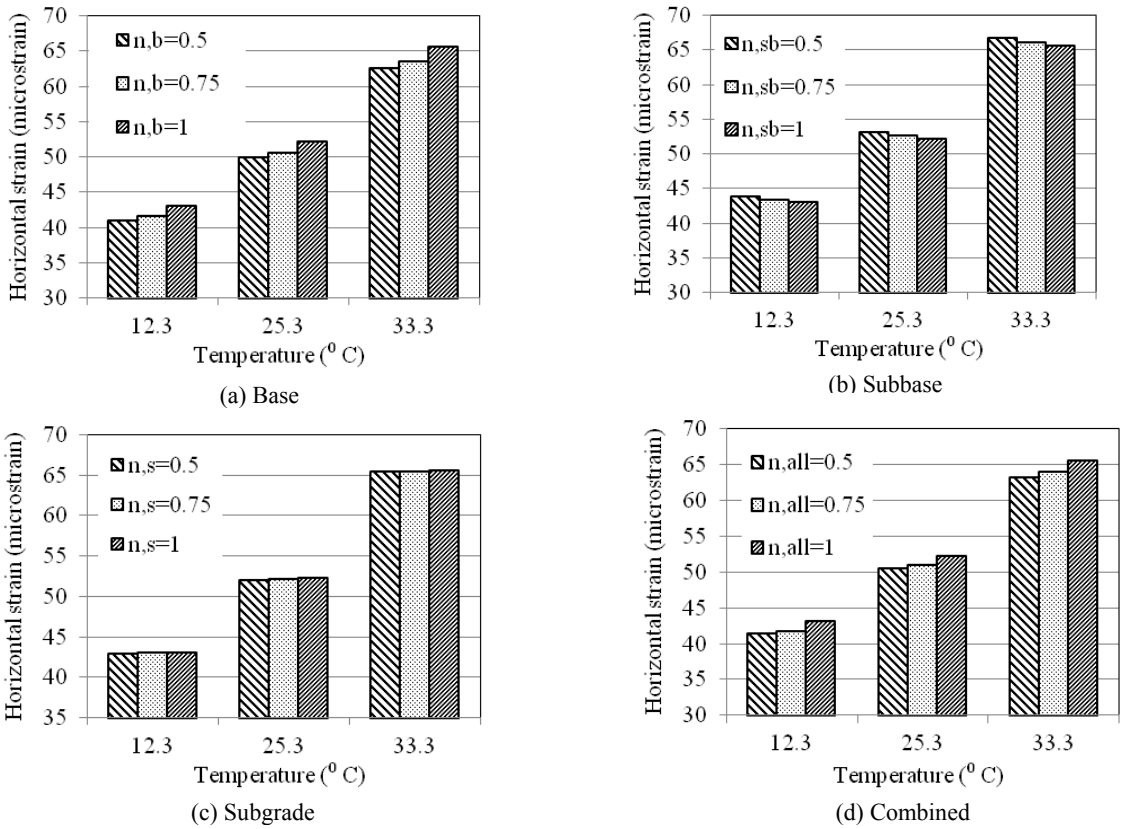

Fig. 5. Effect of Cross-anisotropy on Horizontal Strain at the Bottom of AC Layer.

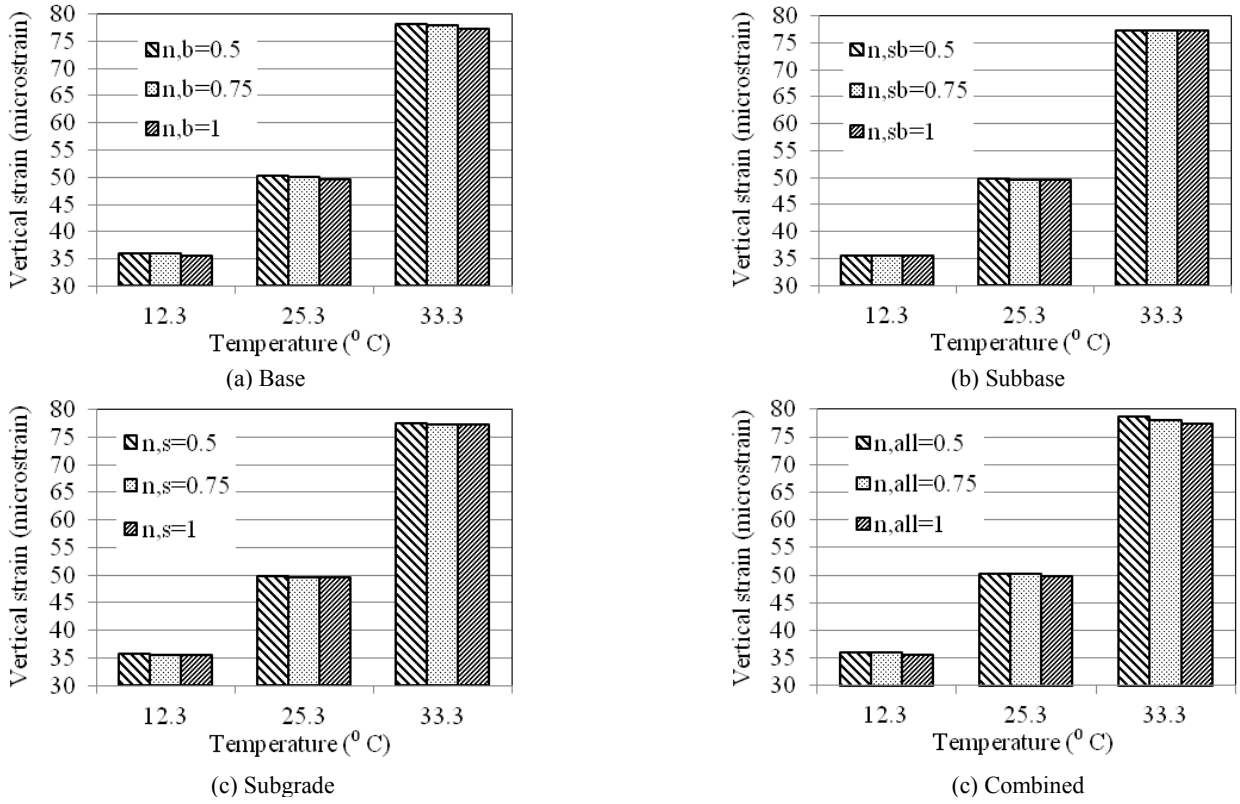

Fig. 6. Effect of Cross-anisotropy on Vertical Strain in AC Layer.

The effect of the subgrade cross-anisotropy on the AC layer horizontal strain is shown in Fig. 5(c). The strain slightly increases with the increase in *n*-value. The variation of strain with change in temperature is still dominant. Compared to the effect of the temperature as well as the former two cases, the effect of the subgrade cross-anisotropy on AC horizontal strain is insignificant.

The effect of cross-anisotropy of all three unbound layers (combined) on the horizontal strain is shown in Fig. 5(d). It is observed that the horizontal strain increases with increase in *n*-value overall. The effect of the base layer cross-anisotropy influences the result the most. In summary, cross-anisotropy of the base layer needs to be considered in pavement analysis and design. This is because the horizontal strain at the bottom of AC layer is related to fatigue cracking of asphalt pavement.

Effect of Cross-Anisotropy on Vertical Strain

The vertical strains are determined at the middle of AC, base, and subbase layer. In the case of subgrade, it is determined at the top. The peak vertical strains are obtained from the time-histories. The *n*-value is kept constant whenever the n-value of an unbound layer is varied.

Fig. 6(a) through 6(d) shows the effect of cross-anisotropy on vertical strain in AC layer. Fig. 6(a) shows that the vertical strain in the AC layer increases rapidly with temperature. It is found to be insensitive to the variation of the *n*-value of the base layer at 12.3°C and 25.3°C.

In Fig. 6(b), the AC strain is fairly constant at all the *n*-values of the subbase layer at different temperatures. Fig. 6(c) shows that the AC strain can be influenced slightly by *n*-values of subgrade at 33.3°C. However, it is not affected by *n*-value at lower temperatures. From Fig. 6(d), it is observed that the combined cross-anisotropy variation has very little influence on vertical strain of the AC layer. In summary, it is observed that vertical strain of the AC layer is barely affected by the cross-anisotropy of unbound layers. It indicates that only temperature affects the permanent deformation in AC layer. Fig. 7(a) through 7(d) shows the effect of cross-anisotropy on vertical strain in the base layer. In Fig. 7(a), it is observed that the base vertical strain is significantly affected by the *n*-value variation of the base layer. Fig. 7(b) shows that the base vertical strain is also affected by the subbase cross-anisotropy.

In case of the subgrade cross-anisotropy, the base vertical strain is slightly influenced by *n*-values as shown in Fig. 7(c). From Fig. 7(d), combined cross-anisotropy affects the vertical strain in the base layer. Among the different cases of cross-anisotropy variation, base layer cross-anisotropy dominantly influences the vertical strain base layer. In all these cases, vertical strain is sensitive to temperature variation. Therefore, in addition to temperature, permanent deformation in base layer is highly sensitive to base layer cross-anisotropy.

Fig. 8(a) through 8(d) shows the effect of cross-anisotropy on vertical strain in the subbase layer. Fig. 8(a) shows that the vertical strain in the subbase layer is significantly affected by the cross-anisotropy of the base layer. Similar to this trend, the vertical subbase strain increases with an increase in *n*-value as shown in Fig. 8(b).

In case of subgrade cross-anisotropy, subbase strain varies with *n*-values as shown in Fig. 8(c). From Fig. 8(d), it is observed that

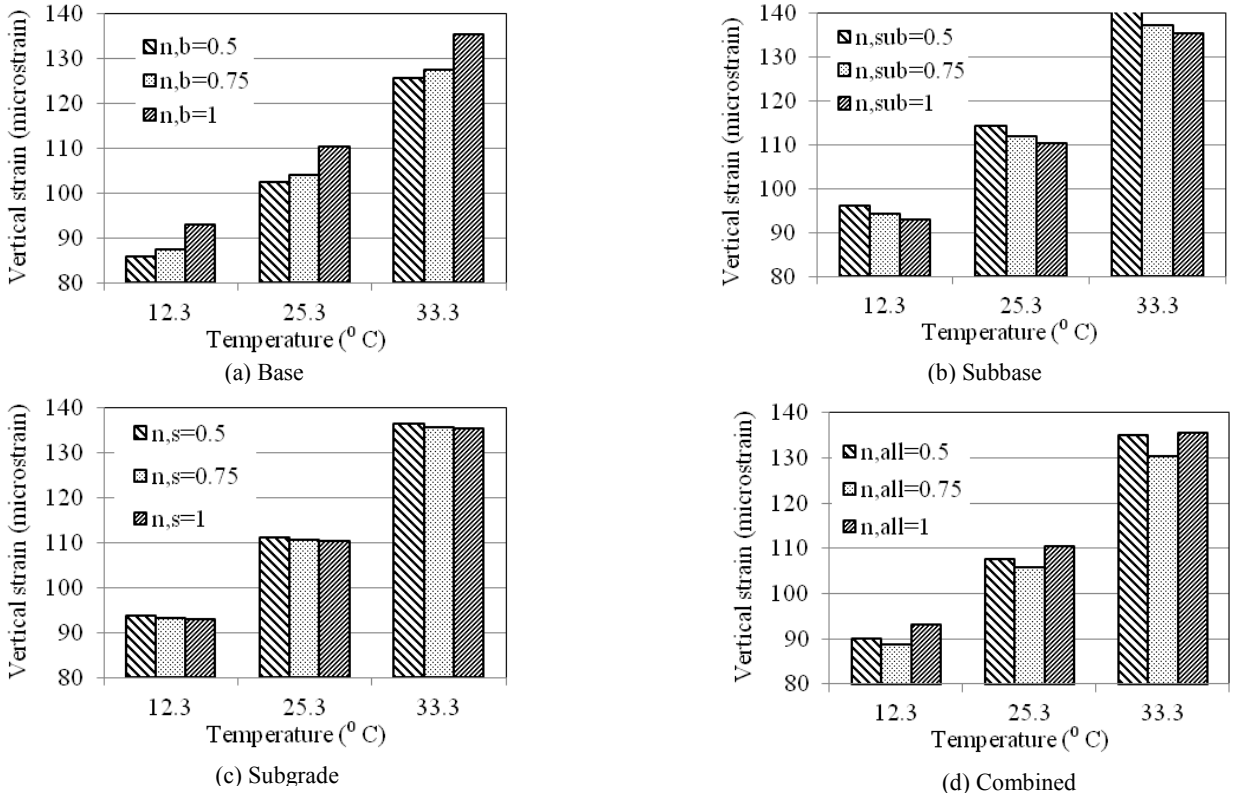

Fig. 7. Effect of Cross-Anisotropy on Vertical Strain in Base Layer.

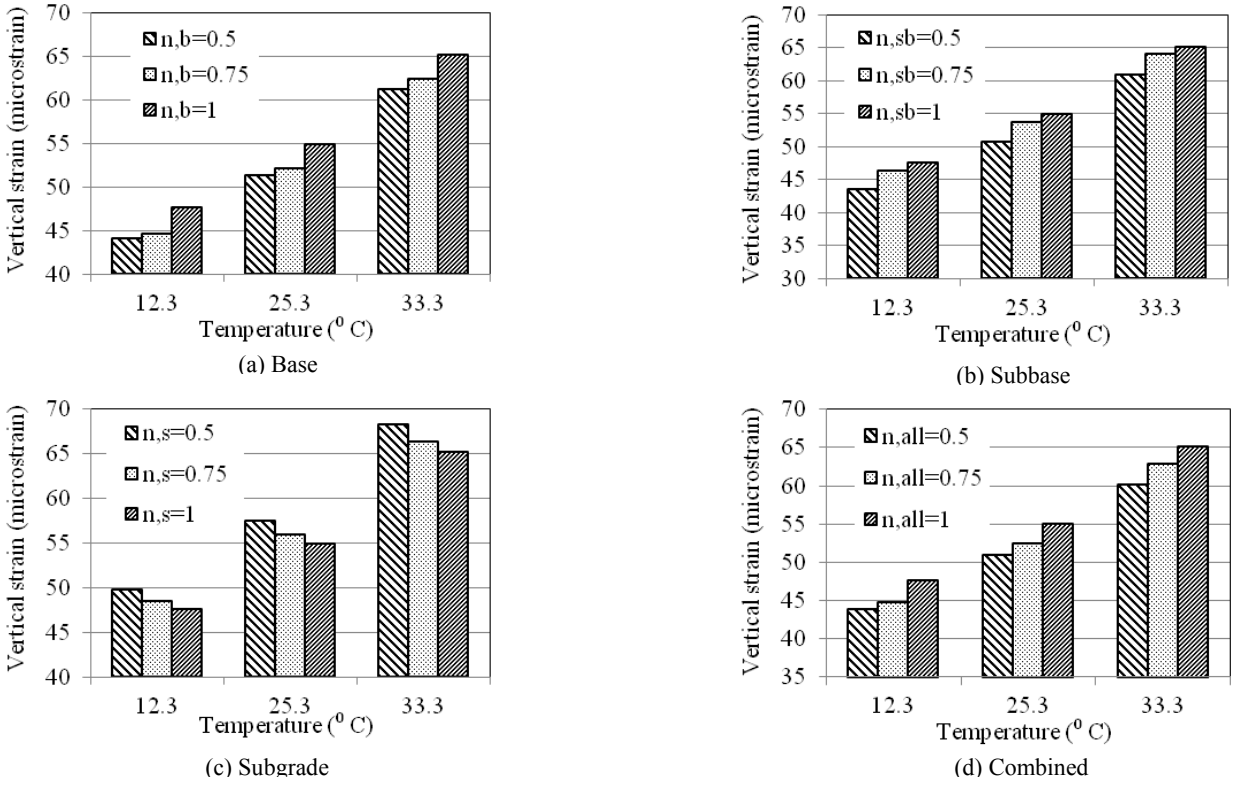

Fig. 8. Effect of Cross-anisotropy on Vertical Strain in Subbase Layer.

the combined cross-anisotropy has significant effect on the vertical strain of the subbase. Finally, it is observed that the vertical strain in subbase is significantly affected by the cross-anisotropy of both base and subbase in addition to the temperature variation.

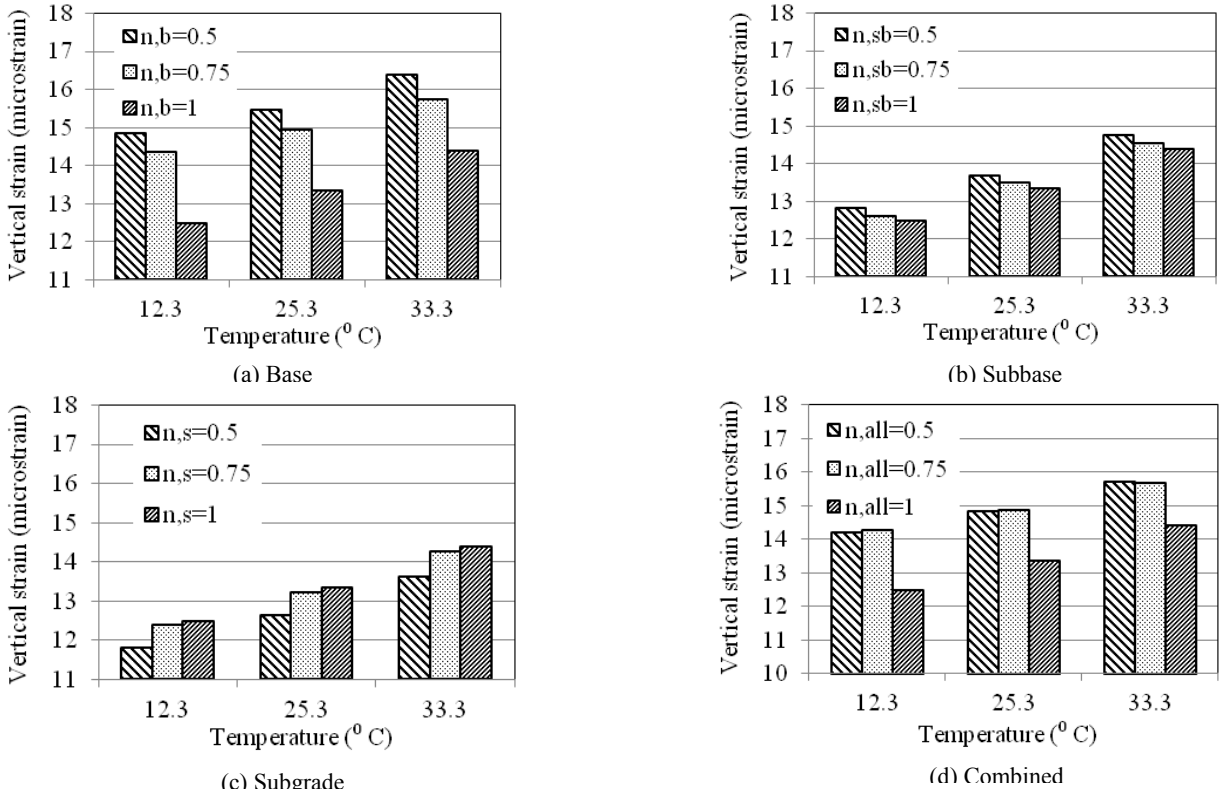

Fig. 9. Effect of Cross-anisotropy on Vertical Strain in Subgrade.

Fig. 9 (a) through 9(d) show the effects of cross-anisotropy on vertical strain on top of the subgrade. Fig. 9(a) shows that subgrade strain is sensitive to the *n*-values of base. In Fig. 9(b), it is observed that the subgrade strain is less sensitive to the subbase cross-anisotropy compared to the case of base cross-anisotropy. Fig. 9(c) shows that the subgrade vertical strain is affected by *n*-values of subgrade though it is small. Similarly, combined cross-anisotropy influences the subgrade vertical strain as shown in Fig. 9(d). In summary, it is obvious that the base cross-anisotropy has a dominant effect on the vertical strain on top of the subgrade. Temperature does not have a pronounced effect on this strain as compared to the earlier cases. Therefore, base layer cross-anisotropy may play an important role in the permanent deformation in subgrade.

Conclusions

The FEM simulation has been performed to determine the horizontal strain at bottom of the AC layer as well as vertical strain in AC, base, subbase, and subgrade for varying degree of cross-anisotropy in unbound layers. Based on the findings from the simulation results, the following conclusions can be made:

- Base layer cross-anisotropy has the most pronounced effect on the horizontal strain at the bottom of the AC layer. The horizontal strain decreases with decrease in *n*-value, i.e., decrease in horizontal modulus of base layer. Incorporation of this variation in horizontal strain to any pavement performance model may lead to a significant variation of pavement performance. Therefore, base layer cross-anisotropy should be considered for fatigue cracking during pavement analysis and design.
- The vertical strain of the AC layer is not sensitive to the cross-anisotropy of unbound layers. It indicates that consideration of vertical strain in AC layer due to incorporation of varying cross-anisotropy of unbound layer in pavement performance model may not significantly affect the permanent deformation of AC layer.
- Vertical strains in the base, subbase, and subgrade layers are significantly affected by cross-anisotropy, except subgrade cross-anisotropy affects the vertical strain slightly. Incorporation of vertical strain in base and subbase due to varying degree of cross-anisotropy to pavement performance may result noticeable amount of permanent deformation in pavement.
- Temperature influences both horizontal strain at the bottom of the AC layer and vertical strains in the unbound layers significantly. Due to the increase in AC layer temperature, both horizontal strain in AC layer as well as vertical strain in AC and unbound layers increases.

The validation of this model with pavement responses from instrumented section under FWD test at different temperatures shows that the materials behaves similar to isotropic material. Finally, it is recommended to perform further study predict the possible presence of cross-anisotropy in the materials.

Acknowledgements

The authors would like to acknowledge the initiative and effort by

Virgil Valdez and James Gallegos, NMDOT personnel, to make the arrangements for the field test on the instrumented section. Special thanks are extended to the members of the NMDOT field exploration team. The effort of Asifur Rahman, a member of the research group, toward the dynamic modulus test is highly appreciated.

References

1. Tutumluer, E., (1998). Anisotropic Behavior of Unbound Aggregate Bases-State of the Art Summary, *Proceedings of the 6th Annual Symposium of the International Center for Aggregate Research*, pp. 11–33, St. Louis, Missouri, USA.
2. Masad, S., Little, D., and Masad. E., (2006). Analysis of Flexible Pavement Response and Performance Using Isotropic and Anisotropic Material Properties, *Journal of Transportation Engineering*, 132 (4), pp. 342–349.
3. Ahmed, M.U., Tarefder, R.A., and Islam, M.R., (2013). Effect of Cross-Anisotropy of AC Modulus on FWD Deflections and Embedded Sensor Stress-Strain, *Transportation Research Record,* No. 2369, pp. 20–29.
4. Wang, H. and Al-Qadi, I.L., (2013). Importance of Nonlinear Anisotropic Modeling of Granular Base for Predicting Maximum Viscoelastic Pavement Responses under Moving Vehicular Loading, *Journal of Engineering Mechanics*, 139(29), pp. 29–38.
5. Robbins, M.M., (2009). An Investigation into Dynamic Modulus of Hot-mix Asphalt and its Contributing Factors, *M.Sc. Thesis*, Auburn University, Auburn, Alabama, USA.
6. Bayat, A., Kasani, H.A., and Soleymani, H.R., (2011). Investigation of Temperature Dependency of Asphalt Concrete Using Laboratory Dynamic Modulus and Field Deflection Testing, *90th Annual Meeting of Transportation Research Board*, pp. 1–14, Washington, DC, USA.
7. Islam, M.R. and Tarefder, R.A., (2013). Evaluating the Longitudinal and the Transverse Horizontal Strains at the Bottom of Hot Mix Asphalt, *International Journal of Science and Engineering Research*, 4 (3), pp. 1–5.
8. Appea, A.K., (2003). Validation of FWD Testing Results Virginia Smart Road: Theoretically and by Instrument Responses, *PhD Dissertation*, Virginia Polytechnic Institute and State University, Blacksburg, Virginia, USA.
9. Choi, J., Seo, Y., Kim, S.H., and Beadles, S., (2011). Flexible Pavement Analysis Considering Temperature Profile and Anisotropy Behavior in Hot Mix Asphalt Layer, *Open Journal of Civil Engineering*, No. 1, pp. 7–12.
10. Al-Qadi, I.L., Wangand, H., and Tutumluer, E., (2010). Dynamic Analysis of Thin Asphalt Pavements Utilizing Cross-Anisotropic Stress-Dependent Properties for Granular Layer, *Transportation Research Record*, No. 2154, pp. 156-163.
11. Oh, J.H., Lytton, R.L., and Fernando, E.G., (2006). Modeling of Pavement Response Using Nonlinear Cross-Anisotropy Approach, *Journal of Transportation Engineering*, 132(6), pp. 458–468.
12. Howard, I.L. and Warren, K.A., (2009). Finite-Element Modeling of Instrumented Flexible Pavements under Stationary Transient Loading, *Journal of Transportation Engineering*, 135(2), pp. 53–61.
13. Schwartz, C.W., (2002). Effect of Stress-Dependent Base Layer on the Superposition of Flexible Pavement Solutions, *International Journal of Geomechanics*, 2(3), pp. 331–352.
14. Petyt, M., (1990). *Introduction to Finite Element Vibration Analysis*, 1st edition, Cambridge University Press, Cambridge, UK.
15. Duncan, J.M., Monsmith, C.L., and Wilson, E.L., (1968). Finite Element Analyses of Pavements, *Highway Research Record*, No. 228, pp. 18–23.
16. Haddad, Y.M., (1995). *Viscoelasticity of Engineering Materials*, 1st edition, Chapman & Hall, New York, USA.
17. Lee, H.J., (1996). Uniaxial Constitutive Modeling of Asphalt Concrete Using Viscoelasticity and Continuum Damage Theory, *PhD Dissertation*, Civil Engineering Department, North Carolina State University, Raleigh, NC, USA.
18. Elseifi, M.A., Al-Qadi, I.L., and Yoo, P.J., (2006). Viscoelastic Modeling and Field Validation of Flexible Pavements, *Journal of Engineering Mechanics*, 132(2), pp. 172–178.
19. AASHTO TP 62-07., (2007). Standard Method of Test for Determining Dynamic Modulus of Hot Mix Asphalt Concrete Mixtures, *AASHTO Provisional Standards*, Washington, DC, USA.
20. Park, S.W. and Schapery, R.A., (1999). Methods of Interconvertion between Linear Viscoelastic Material Functions. Part I- A Numerical Method Based on Prony Series, *International Journal of Solids and Structures*, 36, pp. 1653–1675.
21. AASHTO T307-99., (2003). Standard Method of Test for Determining the Resilient Modulus of Soils and Aggregate Materials, American Association of State Highway and Transportation Officials, Washington, DC, USA.
22. Applied Research Associates (ARA), (2004). Guide for mechanistic-empirical design of new and rehabilitated pavement structures, *NCHRP 1-37A Final Report*, Transportation Research Board, Washington, DC, USA.
23. Kim, S.H., (2004). Determination of Aggregate Physical Properties and its Effect on Cross-Anisotropic Behavior of Unbound Aggregate Materials, *Ph.D. Dissertation*, Texas A&M University, College Station, TX, USA.
24. Hagström, T. and Johansson, M., (2007). Analysis of Inflatable Structures Using ABAQUS/Explicit, MSc Thesis, KTH Engineering Sciences, Stockholm, Sweden.
25. Russell, C. (2005). Deployable Simulation of Inflatable Tensegrity Frameworks, MSc Thesis, Royal Institute of Technology, Department of Mechanics, Stockholm, Sweden.
26. Fekadu, P. (2010). Simulating the Dynamic Response of a Soil-pile System using ABAQUS, MSc Thesis, Department of Civil and Environmental Engineering, Chalmers University of Engineering and Technology, Gothenburg, Sweden.
27. Serdaroglu, M.S., (2010). Nonlinear Analysis of Pile Driving and Ground Vibrations in Saturated Cohesive Soils Using the Finite Element Method, Ph.D. Dissertation, University of Iowa, Iowa City, Iowa, USA.